ChemComm

COMMUNICATION

View Article Online
View Journal | View Issue

Cite this: *Chem. Commun.*, 2025, **61**, 6905

Received 21st February 2025,
Accepted 24th March 2025

DOI: 10.1039/d5cc00971e

rsc.li/chemcomm

Chiral sensing combined with nuclease activity assay to track Cas9 dynamics in solution: ROA and CPL study†

Monika Halat, *[a] Magdalena Klimek-Chodacka, [a] Agnieszka Domagała, [bc] Grzegorz Zając, [b] Tomasz Oleszkiewicz, [a] Josef Kapitán [d] and Rafal Baranski [a]

Chiroptical studies of the SpyCas9 protein are extremely rare. Non-destructive methods are needed to characterize its active ribonucleoprotein form. Using Raman optical activity (ROA) and circularly polarized luminescence (CPL), we present a new approach to detect key biomolecules involved in CRISPR-Cas technology while preserving their original nucleolytic activity.

Since 2012, the use of *Streptococcus pyogenes* SpyCas9 protein has rapidly revolutionized biological sciences[1] as a primary element of site-directed mutagenesis[2] (gene scissors or molecular scalpel technology utilizing CRISPR-Cas system), derived from the adaptive immune response in microbes. Given the growing interest in exploiting the CRISPR-Cas mechanism, there is an urgent need for efficient detection of active and stable ribonucleoprotein complexes (RNP) enabling targeting and cutting of any predefined DNA region under physiological conditions. For this reason, Raman optical activity (ROA) was applied and complemented by nuclease activity assay, including the induction of DNA cleavage *in vitro*[3] and in living cells,[4] and the determination of the size of the obtained FAM-labelled DNA fragments using capillary electrophoresis (see Table S2 and Fig. S1, S2 of the ESI†).

ROA enables the study of protein structure in aqueous solution,[5] which is a significant advantage over the more popular X-ray crystallography,[6] and, unlike NMR spectroscopy, directly reflects rapid conformational changes.[7] By recording a small difference in the intensity of Raman scattered light for the right and left circular polarization ($I_R - I_L$),[8] ROA provides detailed insight into the protein geometry, such as secondary and tertiary elements,[9] backbone hydration,[10] side-chain conformation,[11] and structural arrangements present in the unfolded state (polyproline II helix, PPII).[12] It is more sensitive to 3D structure than electronic circular dichroism (ECD) by reporting chirality associated with vibrational transitions of molecules.[2] ROA of proteins has evolved over the years – from simple polypeptides measured in the 1990s[13] to the more complex targets studied today, such as glycoproteins,[14] photoreceptor proteins,[15] blood plasma,[16] and amyloid fibrils.[17] Moreover, the ROA effect can be successfully combined with circularly polarized luminescence (CPL), which is known as the ROA-CPL approach.[18] This method requires the use of luminescent probes, *e.g.* Eu(III) complexes, whose chirality is induced by interactions with optically active components, such as peptides,[19] proteins[20] or DNA.[21] Matching the energy of the ROA excitation line (532 nm) to the electronic transition of the Eu(III)-based probe gives rise to an enhanced CPL signal sensitive to the local chiral environment, here the SpyCas9 nuclease and its RNP complex (Fig. 1).

Therefore, we present the first, to our knowledge, ROA study combined with Eu(III)-CPL probing identifying major changes

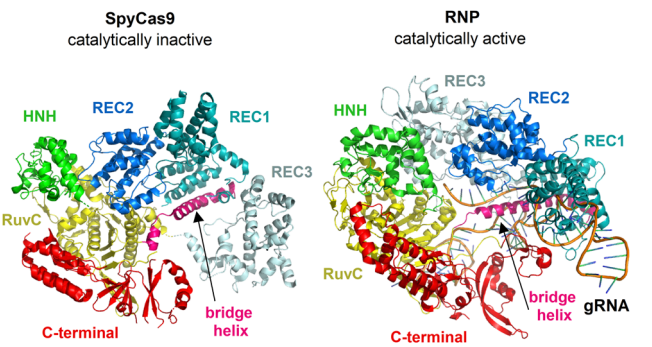

Fig. 1 Overall structure of SpyCas9 (PDB ID: 4CMP)[22a] and RNP (PDB ID: 4ZT0)[22b] shown in ribbon representation.

[a] *Department of Plant Biology and Biotechnology, Faculty of Biotechnology and Horticulture, University of Agriculture in Krakow, AL. Mickiewicza 21, 31-120 Krakow, Poland. E-mail: m.halat@urk.edu.pl*
[b] *Jagiellonian Centre for Experimental Therapeutics (JCET), Bobrzynskiego 14, 30-348 Krakow, Poland*
[c] *Doctoral School of Exact and Natural Sciences, Jagiellonian University, Prof. S. Łojasiewicza 11, 30-348 Krakow, Poland*
[d] *Department of Optics, Palacký University Olomouc, 17. listopadu 12, 77146, Olomouc, Czech Republic*

† Electronic supplementary information (ESI) available. See DOI: https://doi.org/10.1039/d5cc00971e

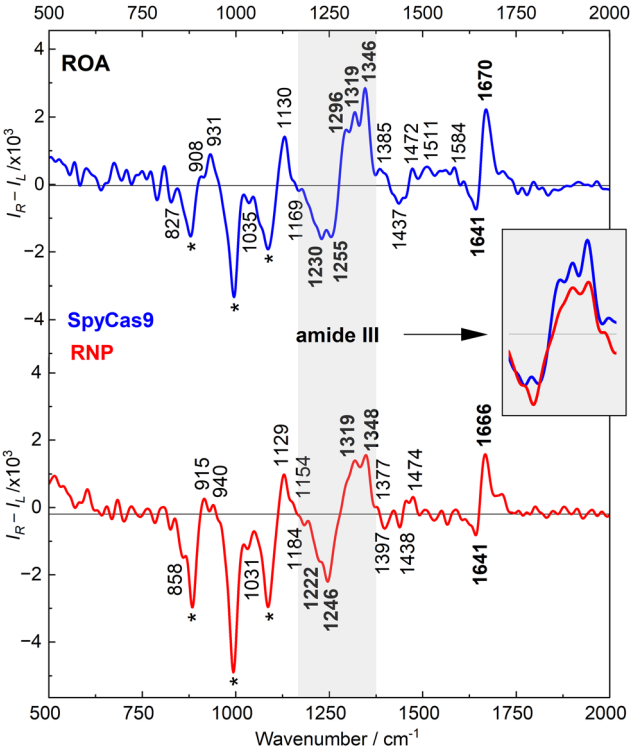

Fig. 2 ROA spectra of SpyCas9 protein (blue) and its active RNP complex (red). Asterisks were assigned to the buffer bands (see Fig. S3, S4 and Table S3, ESI†).

in the geometry of SpyCas9 enzyme during its catalytic activation, *i.e.* upon binding of a short oligonucleotide guide RNA (gRNA). Finally, we propose two biologically neutral ROA-CPL sensors: $[Eu(DPA)_3]^{3-}$ and $EuEDTA^-$, intended to detect initially inactive and activated forms of the SpyCas9 in solution, without the need for further genetic testing.

As shown in Fig. 2, ROA spectra of the SpyCas9 (blue) and its RNP (red) expose chiral signatures that can be directly assigned to a proper secondary structure. The first one is the amide I couplet originating from the C=O stretching vibrations of the peptide bond. In both cases the couplet is centered at ~1650 cm^{-1} with the −/+ pattern of bands, indicating the right-handed α-helix.[5a,9a,9d] Crystallographic data[22] confirms that the SpyCas9 is a bi-lobed α-rich nuclease (49.6%)[23] featuring also mixed α/β domains (Fig. 1). The same order of bands is also observed for β-proteins, but it is typically shifted by ~10 cm^{-1} towards higher wavenumbers.[5a,9a,9d] Spectral variations in the amide I range may signify some rearrangements in a protein structure. However, both ROA couplets reveal similar intensities and frequencies, regardless of whether the gRNA is attached to SpyCas9 or not.

The most noticeable ROA differences induced by the active RNP formation arise from the extended amide III range: ~1230–1350 cm^{-1}, dominated by the coupled N–H and Cα–H deformations (Fig. 2, grey background). The −/+/+ pattern observed at 1255/1296/1346 cm^{-1} in the SpyCas9 spectrum is very sensitive to change in the α-helical conformation.[10c,11a,12a] There is a decrease in the intensity of the +1296 cm^{-1} band, which is practically invisible in the RNP profile. This marker strongly depends on the backbone geometry, defined by the two torsion angles ϕ and ψ, which can be affected by intramolecular hydrogen bonding or interaction with the solvent.[10b,10c,12a] ROA simulations proved that the + intensity at ~1300 cm^{-1} collapses for structures with ϕ, ψ values in the bottom right of the α-helical region of the Ramachandran plot (ϕ, ψ = −59°, −44°; ϕ, ψ = −55°, −53°) or with increasing conformational freedom.[10c,12a] The ROA signal at +1346 cm^{-1} is more resistant to different ϕ, ψ combinations and is considered a robust signature of the regular α-helix (ϕ, ψ = −66°, −41°).[10c,12a] However, its intensity may be lower when the classical α-structure unfolds into an extended PPII formation (ϕ, ψ = −75°, 145°).[5a,12a] Since the ROA +1319 cm^{-1} band is characteristic of the PPII element and occurs in the RNP spectrum with a clearly less intense +1348 cm^{-1} band, such interconversion is possible. Comparing the intensity ratios of the 1319/1348 cm^{-1} bands before and after nuclease activation, it appears that the PPII content slightly increases upon gRNA binding. The PPII hydration manner makes the structure very flexible and highly exposed to the solvent.[24] Typically, PPIIs participate in numerous protein–protein and protein–nucleic acid interactions, acting as peptide ligands or forming structural binding motifs. It follows, that PPII helices may have a significant role during the SpyCas9 → RNP transition. In fact, when gRNA associates, the α-helical lobe of SpyCas9 (REC lobe, Fig. 1) undergoes serious conformational alternations.[22a,25] The number of internal hydrogen bonds decreases reducing the folding of the protein structure – the percentage of helical elements drops by a total of 5% in favor of a rise in dynamic residues (up to 20% in the REC2 domain).[25b] Hence, the sensitivity of ROA to distinguish two positive amide modes with Cα–H bending perpendicular (~1300 cm^{-1}) or parallel (~1345 cm^{-1}) to the Cα–N bond, is extremely valuable in tracking structural heterogeneity of α-helical sequences in solution.[10b,c,12a] This is a great advantage over the ECD study, which only showed a general decrease in SpCas9 α-helicity upon gRNA binding.[23]

The negative part of the amide III range is strongly dependent on the orientation of the protein side chains.[11] The nuclease bridge helix (Fig. 1) contains eight positively charged arginine (Arg) residues that are crucial for establishing contact with the negatively charged gRNA backbone.[25b,26] The shift down in wavenumbers of the −1255 → −1246 cm^{-1} band (Fig. 2) may be attributed to the different Arg rotamers,[11a] determined, by the side-chain dihedral angles: χ_1 = 180°(*trans*) → χ_1 = −60°(*gauche*−). The average impute of hydrophobic residues to the amide III profile should also be taken into account,[11a] since their side chains exposure expands after RNP complexation.[25b] The spectral variation observed within the second negative amide III mode (−1230 → −1222 cm^{-1}) may be related to rearrangements in domains containing β-motifs (Fig. 1, RuvC and C-terminal parts[22a,25]). In early ROA experiments, the ROA feature at ~1220 cm^{-1} was proposed as a characteristic of the β-turn moiety.[5a,9d] However, recent calculations have canceled this assignment as it may be affected by the conformation of other secondary structures.[11b] Nevertheless. upon interaction with gRNA, the amount of β-sheets decreases and β-turns increases by about several %,[25b] which may generate the down-shift of this ROA band.

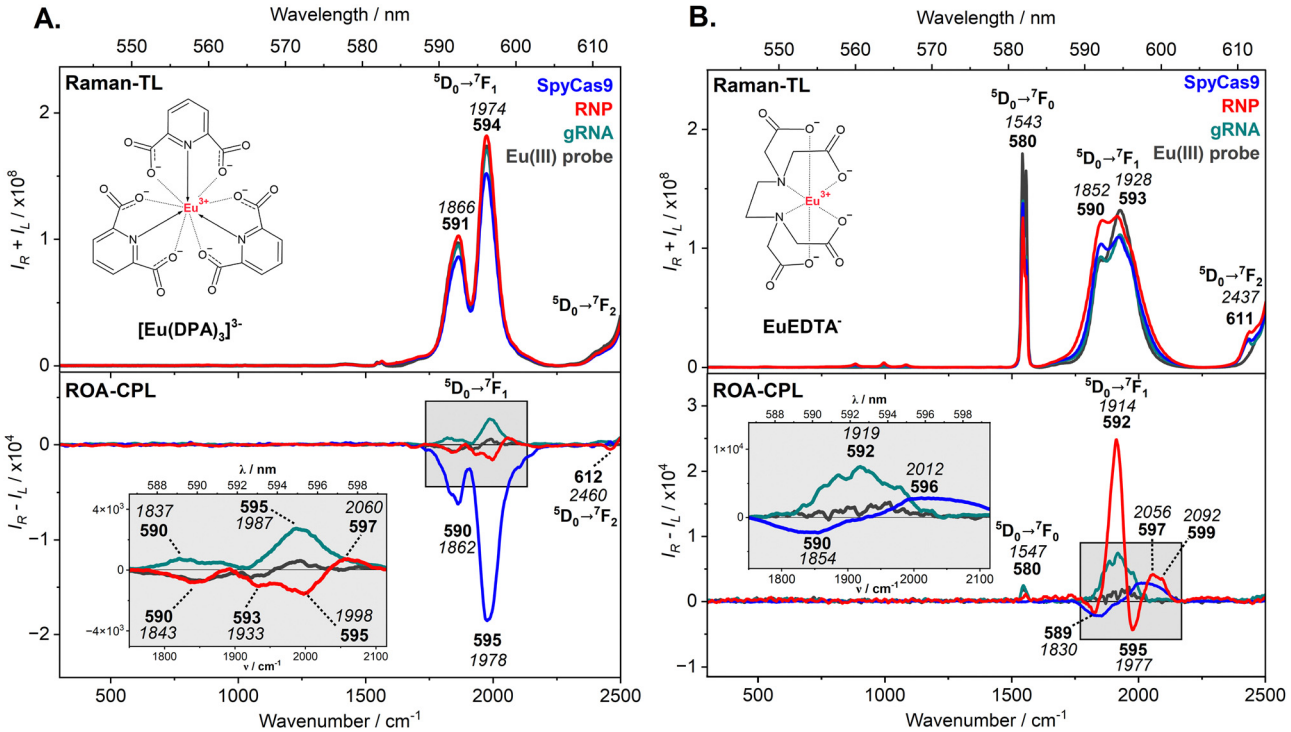

Fig. 3 Raman-TL and ROA-CPL spectra of SpyCas9 (blue), RNP (red), and gRNA (green), combined with $[Eu(DPA)_3]^{3-}$ (panel A) and $EuEDTA^-$ (panel B), and of the free Eu(III)-probe (dark grey). Luminescent bands were expressed in nm (bold) and cm^{-1} (italic) scales.

An alternative method to confirm successful RNP complexation is the ROA-CPL approach using two non-chiral probes: $[Eu(DPA)_3]^{3-}$ and $EuEDTA^-$ (Fig. 3). The Raman and ROA spectra are dominated by the total luminescence (TL) and CPL bands, respectively, assigned to selected electronic transitions of Eu(III).[27] Vibrational bands of studied molecules are invisible due to their low concentrations (6.1 μM). The vibrational bands of the probes are also not recognizable under the 532 nm excitation line.[28] Each achiral, racemic Eu(III)-complex (2 mM) generates a characteristic spectroscopic response under the chiral influence of SpyCas9, gRNA, and RNP (chirality induction phenomenon), without changing their catalytic activity (see Fig. S1 and Table S2, ESI†). Therefore, ROA-CPL spectra are much more informative and allow for detecting differences between those species, while Raman-TL spectra reveal identical profiles, perfectly matching the spectrum of a single Eu(III)-probe.

As presented in Fig. 3A, the most intense TL and CPL bands are associated with the $^5D_0 \rightarrow {}^7F_1$ transition (590–595 nm). The $^5D_0 \rightarrow {}^7F_0$ transition (~580 nm) is barely seen, because it is forbidden by the selection rules for high-symmetry complexes such as $[Eu(DPA)_3]^{3-}$ (D_3 symmetry).[27b] Next, the $^5D_0 \rightarrow {}^7F_2$ transition (over 613 nm) is cut off at the very beginning, due to the limited spectral range. The CPL patterns induced by the SpyCas9 protein, gRNA, and their active RNP form differ in terms of signs and the number of bands, due to different chirality and interaction sites of the measured species, which differently disturb the enantiomeric equilibrium ($\Lambda \leftrightarrow \Delta$) of the $[Eu(DPA)_3]^{3-}$ probe (Pfeifer effect).[20b,29] Their individual CPL response can also be quantified by the circular intensity difference (CID values, Table S5, ESI†), *i.e.* the ratio of ROA-CPL ($I_R - I_L$) to Raman-TL ($I_R + I_L$) spectra. The negative CPL profile of the SpyCas9 nuclease suggests that one of the $[Eu(DPA)_3]^{3-}$ enantiomers predominates in the solution. Adequately, CID values for these bands are relatively high ($\sim 10^{-4}$) compared to those calculated for gRNA and RNP ($\sim 10^{-6}$–10^{-5}). The $[Eu(DPA)_3]^{3-}$ probe is more efficient in detecting the SpyCas9 structure without destroying its dedicated nucleolytic activity (Table S2 and Fig. S1, ESI†). Low-intensity CPL bands for gRNA and RNP are just above the ROA detection limit, thus, it is recommended to use another Eu(III)-probe to easily distinguish them in solution.

The $EuEDTA^-$ complex possesses three vacancies in the inner coordination sphere,[30] so it behaves differently under the influence of chiral agents, which not only disturb its enantiomeric equilibrium ($\Lambda \leftrightarrow \Delta$) but can also bind to its central Eu(III) ion. Fig. 3B shows the Raman-TL and ROA-CPL spectra of SpyCas9, gRNA, and RNP probed with the $EuEDTA^-$, where the luminescent signals of the sensor are dominant. Again, all TL profiles are quite similar and only the ROA spectra provide very distinctive CPL bands in the range of $^5D_0 \rightarrow {}^7F_1$ transition (589–599 nm). The most intense CPL response was registered for the RNP form suggesting the strongest interaction to the $EuEDTA^-$. Its bisignate pattern of multiple CPL bands is characterized by high CID ratios ($\sim 10^{-4}$, Table S5, ESI†), up to 100 times higher in comparison to the previous $[Eu(DPA)_3]^{3-}$ probing. The $EuEDTA^-$ complex sensitively recognizes the RNP complex at very low concentrations (6.1 μM), maintaining the programmed catalytic activity (Table S2 and Fig. S1, ESI†). SpyCas9 and gRNA treated separately with $EuEDTA^-$ do not generate as strong CPL response

as their active combination (CID values $\sim 10^{-6}$–10^{-5}). However, their CPL patterns look different, the −/+ couplet for SpyCas9 and the single positive band for gRNA are observed.

In summary, we employed ROA combined with Eu(III)-CPL probing as an effective approach to identify structural rearrangements in the SpyCas9 geometry upon gRNA binding in solution. Through an advanced activity assay, we confirmed the harmlessness of ROA and the neutral nature of Eu(III)-based probes regarding the original properties of the CRISPR-related biomolecules. The most informative ROA region was the amide III range, which revealed changes in the conformation of the α-helical backbone, an increase in PPII content, and the orientation of Arg side chains. The obtained CPL patterns were distinctive, enabling clear differentiation between inactive and active nuclease forms. $[Eu(DPA)_3]^{3-}$ exhibited a stronger affinity for SpyCas9, while $EuEDTA^-$ was more suitable for RNP detection. We found $EuEDTA^-$ to be a promising sensor for tracking catalytically active RNPs at low concentrations (<6.1 μM) without the need for complex genetic assays.

Funding was provided by the National Science Centre (NCN) under grants no. 2021/40/C/ST4/00190 to M.H. (SpyCas9 purchase, gRNA and RNPs synthesis, ROA/CPL measurements and analysis, nuclease activity assay) and 2019/35/B/ST4/04161 to G.Z. (providing Eu(III)-based probes, ROA/CPL analysis).

Data availability

All data are available in the main text or the ESI.† Data are also available upon request to the corresponding author.

Conflicts of interest

The authors declare no competing interests.

Notes and references

1 M. Jinek, K. Chylinski, I. Fonfara, M. Hauer, J. A. Doudna and E. Charpentier, *Science*, 2012, **337**, 816–821.
2 C. Zhang, Z. Huang, Z. Li, J. Hu, R. Liu and Y. Lv, *TrAC, Trends Anal. Chem.*, 2024, **170**, 117431.
3 M. Klimek-Chodacka, T. Oleszkiewicz, L. G. Lowder, Y. Qi and R. Baranski, *Plant Cell Rep.*, 2018, **37**, 575–586.
4 M. Klimek-Chodacka, M. Gieniec and R. Baranski, *Int. J. Mol. Sci.*, 2021, **22**, 10740.
5 (*a*) T. Fujisawa, *Encyclopedia of Analytical Chemistry: Applications, Theory and Instrumentation*, John Wiley & Sons, 2020, 1–19; (*b*) F. Zhu, N. W. Isaacs, L. Hecht and L. D. Barron, *Structure*, 2005, **13**, pp. 1409–1419.
6 (*a*) M. L. Pusey, Z.-J. Liu, W. Tempel, J. Praissman, D. Lin, B. C. Wang, J. A. Gavira and J. D. Ng, *Prog. Biophys. Mol. Biol.*, 2005, **88**, 359–386; (*b*) K. R. Acharya and M. D. Lloyd, *Trends Pharmacol. Sci.*, 2005, **26**, 10–14.
7 (*a*) M. Buděšínský, P. Daněček, L. Bednárová, J. Kapitán, V. Baumruk and P. Bouř, *J. Phys. Chem. A*, 2008, **112**, 8633–8640; (*b*) S. C. Sue, C. F. Chang, Y. T. Huang, C. Y. Chou and T. Huang, *Phys. A: Stat. Mech. Appl.*, 2005, **350**, 12–27.
8 L. D. Barron, L. Hecht, I. H. McColl and E. W. Blanch, *Mol. Phys.*, 2004, **102**, 731–744.
9 (*a*) C. Mensch, A. Konijnenberg, R. Van Elzen, A.-M. Lambeir, F. Sobott and C. Johannessen, *J. Raman Spectrosc.*, 2017, **48**, 910–918; (*b*) J. Kessler, J. Kapitán and P. Bouř, *J. Phys. Chem. Lett.*, 2015, **6**, 3314–3319; (*c*) A. N. L. Batista, J. M. Batista, V. S. Bolzani, M. Furlan and E. W. Blanch, *Phys. Chem. Chem. Phys.*, 2013, **15**, 20147–20152; (*d*) L. D. Barron, L. Hecht, E. W. Blanch and A. F. Bell, *Prog. Biophys. Mol. Biol.*, 2000, **73**, 1–49.
10 (*a*) S. Yamamoto and F. Kimura, *Phys. Chem. Chem. Phys.*, 2022, **24**, 3191–3199; (*b*) C. Mensch, P. Bultinck and C. Johannessen, *Phys. Chem. Chem. Phys.*, 2019, **21**, 1988–2005; (*c*) C. Mensch, L. D. Barron and C. Johannessen, *Phys. Chem. Chem. Phys.*, 2016, **18**, 31757–31768.
11 (*a*) C. Mensch and C. Johannessen, *ChemPhysChem*, 2019, **20**, 42–54; (*b*) C. Mensch and C. Johannessen, *ChemPhysChem*, 2018, **19**, 3134–3143.
12 (*a*) C. Mensch, P. Bultinck and C. Johannessen, *ACS Omega*, 2018, **3**, 12944–12955; (*b*) C. Johannessen, J. Kapitán, H. Collet, A. Commeyras, L. Hecht and L. D. Barron, *Biomacromolecules*, 2009, **10**, 1662–1664; (*c*) C. D. Syme, E. W. Blanch, C. Holt, R. Jakes, M. Goedert, L. Hecht and L. D. Barron, *Eur. J. Biochem.*, 2002, **269**, 148–156.
13 L. D. Barron, Z. Q. Wen and L. Hecht, *J. Am. Chem. Soc.*, 1992, **114**, 784–786.
14 L. Ashton, P. D. A. Pudney, E. W. Blanch and G. E. Yakubov, *Adv. Colloid Interface Sci.*, 2013, **199–200**, 66–77.
15 J. Matsuo, T. Kikukawa, T. Fujisawa, W. D. Hoff and M. Unno, *J. Phys. Chem. Lett.*, 2020, **11**, 8579–8584.
16 O. Vrtělka, K. Králová, M. Fousková, L. Habartová, P. Hříbek, P. Urbánek and V. Setnička, *Analyst*, 2023, **148**, 2793–2800.
17 (*a*) A. Kolodziejczyk, L. A. Nafie, A. Wajda and A. Kaczor, *Chem. Commun.*, 2023, **59**, 10793–10796; (*b*) A. Kurochka, J. Průša, J. Kessler, J. Kapitán and P. Bouř, *Phys. Chem. Chem. Phys.*, 2021, **23**, 16635–16645.
18 T. Wu, *Phys. Chem. Chem. Phys.*, 2022, **24**, 15672–15686.
19 A. Domagała, S. Buda, M. Baranska and G. Zając, *Spectrochim. Acta A Mol. Biomol. Spectrosc.*, 2025, **324**, 124995.
20 (*a*) M. Krupová, J. Kapitán and P. Bouř, *ACS Omega*, 2019, **4**, 1265–1271; (*b*) T. Wu, J. Kessler and P. Bouř, *Phys. Chem. Chem. Phys.*, 2016, **18**, 23803–23811.
21 T. Wu, P. Bouř and V. Andrushchenko, *Sci. Rep.*, 2019, **9**, 1068.
22 (*a*) M. Jinek, F. Jiang, D. W. Taylor, S. H. Sternberg, E. Kaya, E. Ma, C. Anders, M. Hauer, K. Zhou, S. Lin, M. Kaplan, A. T. Iavarone, E. Charpentier, E. Nogales and J. A. Doudna, *Science*, 2014, **343**, 1247997; (*b*) F. Jiang, K. Zhou, L. Ma, S. Gressel and J. A. Doudna, *Science*, 2015, **348**, 1477–1481; (*c*) H. Nishimasu, F. A. Ran, P. D. Hsu, S. Konermann, S. I. Shehata, N. Dohmae, R. Ishitani, F. Zhang and O. Nureki, *Cell*, 2014, **156**, 935–949.
23 M. Halat, M. Klimek-Chodacka, J. Orleanska, M. Baranska and R. Baranski, *Int. J. Mol. Sci.*, 2021, **22**, 1–14.
24 (*a*) A. A. Adzhubei, M. J. E. Sternberg and A. A. Makarov, *J. Mol. Biol.*, 2013, **425**, 2100–2132; (*b*) P. Kumar and M. Bansal, *J. Struct. Biol.*, 2016, **196**, 414–425.
25 (*a*) F. Jiang and J. A. Doudna, *Annu. Rev. Biophys.*, 2017, **46**, 505–529; (*b*) G. Panda and A. Ray, *Comput. Struct. Biotechnol. J.*, 2022, **20**, 4172–4184.
26 M. Bratovič, I. Fonfara, K. Chylinski, E. J. C. Gálvez, T. J. Sullivan, S. Boerno, B. Timmermann, M. Boettcher and E. Charpentier, *Nat. Chem. Biol.*, 2020, **16**, 587–595.
27 (*a*) A. T. Frawley, R. Pal and D. Parker, *Chem. Commun.*, 2016, **52**, 13349–13352; (*b*) K. Binnemans, *Coord. Chem. Rev.*, 2015, **295**, 1–45.
28 T. Wu, P. Bouř, T. Fujisawa and M. Unno, *Adv. Sci.*, 2024, **11**, 2305521.
29 (*a*) P. Gawryszewska, J. Legendziewicz, Z. Ciunik, N. Esfandiari, G. Muller, C. Piguet, M. Cantuel and J. P. Riehl, *Chirality*, 2006, **18**, 406–412; (*b*) S. Wu, G. L. Hilmes and J. P. Riehl, *J. Phys. Chem.*, 1989, **93**, 2307–2310.
30 (*a*) M. S. Thomsen, P. R. Nawrocki, N. Kofod and T. J. Sørensen, *Eur. J. Inorg. Chem.*, 2022, e202200334; (*b*) T. Wu, J. Průša, J. Kessler, M. Dračínský, J. Valenta and P. Bouř, *Anal. Chem.*, 2016, **88**(8), 8878–8885.

